Macromolecules

ARTICLE

pubs.acs.org/Macromolecules

From Microphase Separation to Self-Organized Mesoporous Phenolic Resin through Competitive Hydrogen Bonding with Double-Crystalline Diblock Copolymers of Poly(ethylene oxide-*b*-ε-caprolactone)

Jheng-Guang Li, Yu-De Lin, and Shiao-Wei Kuo*

Department of Materials and Optoelectronic Science, Center for Nanoscience and Nanotechnology, National Sun Yat-Sen University, Kaohsiung, 804, Taiwan

Supporting Information

ABSTRACT: A series of immiscible crystalline−crystalline diblock copolymers, poly(ethylene oxide)-*b*-(ε-caprolactone) (PEO-*b*-PCL), were synthesized through ring-opening polymerization and then blended with phenolic resin. FT-IR analyses demonstrate that the ether group of PEO is a stronger hydrogen-bond acceptor with the hydroxyl group of phenolic resin than is the carbonyl group of PCL. Phenolic, after being cured with hexamethylenetetramine (HMTA), results in the excluded and confined PCL phase based on analyses by differential scanning calorimetry (DSC). This effect leads to the formation of a variety of composition-dependent nanostructures, including disorder, gyroid and short-cylinder structures. The self-organized mesoporous phenolic resin was found only at 40−60 wt % phenolic content by an intriguing balance of the contents of phenolic, PEO, and PCL. In addition, the mesoporous structure was destroyed at higher PCL/PEO ratios in the block copolymers, as determined by small-angle X-ray scattering (SAXS) and transmission electron microscopy (TEM) experiments. In addition, the large and long-range order of bicontinuous gyroid-type mesoporous carbon was obtained from mesoporous gyroid phenolic resin calcined at 800 °C under nitrogen.

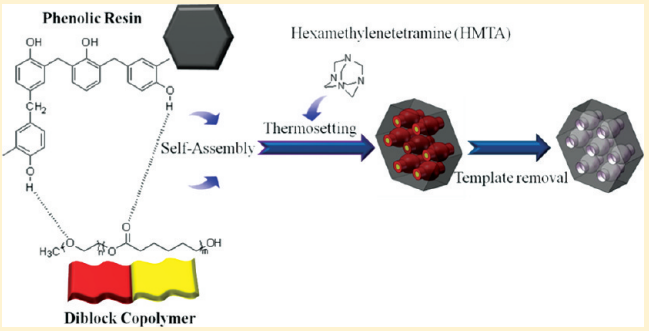

INTRODUCTION

Block copolymers are especially good candidates for the production of self-assembled materials and nanometer-scale devices with a wide range of structural applications, such as the formation of advanced materials, pollution control, and drug delivery.[1,2] Diblock copolymers can form many different well-defined, self-assembled nanostructures in the bulk state, including lamellar, gyroid, hexagonally packed cylinders, hexagonally perforated layers (HPL), ordered bicontinuous double diamond (OBDD), and spherical structures. The formation of these structures results from the presence of two immiscible polymer chains connected by covalent bonds. The structures formed depend on the relative volume fractions of the blocks, the total degree of polymerization, and the Flory−Huggins interaction parameter.[3−6]

Recently, diblock copolymers (A-*b*-B) blended with homopolymers have attracted great interest in polymer science because of their unusual phase behavior.[7−21] Most studies have concentrated on mixing immiscible A-*b*-B diblock copolymers with an A homopolymer, such as homopolymer PS, and styrenic block copolymers. The morphologies of these copolymers strongly depend on the molecular weight of PS homopolymers.[22−32] Another major system that has been investigated is the blending of a homopolymer C with immiscible A-*b*-B diblock copolymer. For an A-*b*-B/C blend system, two different outcomes are possible when C is miscible with immiscible A-*b*-B segments.[32−37] In the first case, C is miscible with B but immiscible with A. Zhao et al. investigated blends of poly(styrene-*b*-vinylphenol) (PS-*b*-PVPh) diblock copolymers with various hydrogen-bond-acceptor polymers, such as poly(ethylene oxide) (PEO), poly(4-vinylpyridine) (P4VP), and poly(butyl methacrylate) (PBMA). The PEO, P4VP and PBMA can form hydrogen bonds with the PVPh block while being immiscible with the PS block, and microphase separation is expected in such systems.[38] Ikkala prepared blends of the polyisoprene-*b*-poly(2-vinylpyridine) (PI-*b*-P2VP) diblock copolymer with novolac phenolic resin, which is miscible with P2VP through hydrogen bonding but immiscible with PI.[39,40] Matsushita studied the various microphase separation structures of a poly(vinylphenol) (PVPh)/poly(styrene-*b*-2-vinylpyridine) (PS-*b*-P2VP) blend system, in which PVPh and P2VP are miscible through strong hydrogen bonding.[41,42] Chet et al. have reported that the ratio of the inter-association equilibrium constant (K_A) to the self-association

Received: May 10, 2011
Revised: October 26, 2011
Published: November 15, 2011

Scheme 1. Preparation of Mesoporous Phenolic Resins

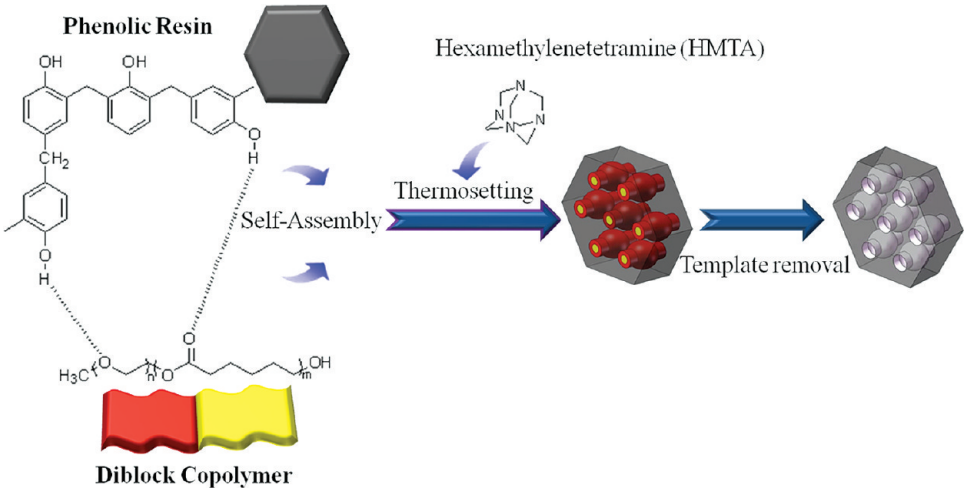

equilibrium constant (K_B), K_A/K_B, is a convenient guide for estimating the phase behavior of A-*b*-B/C. When the K_A/K_B ratio much is larger than unity, such as occurs in the PS-*b*-PVPh/P4VP blend, the system tends to behave as a neat copolymer; when the K_A/K_B ratio is significantly smaller than unity, such as occurs in PS-*b*-PVPh/poly(methyl methacraylte) (PMMA), phase separation instead of order−order phase transitions can be expected when the volume fraction of the homopolymer additive exceeds a certain level.[43]

In the second case, C is miscible with both A and B. For example, Kwei et al. investigated blends of PS-*b*-PVPh/poly(vinyl methyl ether), (PVME), in which PVME is miscible with both the PS and PVPh blocks and serves as a common solvent.[38] Guo and Chen also reported blends of an immiscible A-*b*-B diblock copolymer with C, where C is miscible with both blocks A and B, but the hydrogen-bonding interactions between the B and C segments are stronger than those between the A and C segments ($\chi_{BC} \gg \chi_{AC}$). They found that both blocks of poly(ε-caprolactone)-*b*-poly(4-vinylpyridine) (PCL-*b*-P4VP) and poly(ethylene oxide)-*b*-poly(ε-caprolactone) (PEO-*b*-PCL) interacted with PVPh, poly(acrylic acid) (PAA), and phenoxy resin through hydrogen bonding, where both χ_{AC} and χ_{BC} were negative but χ_{AC} was more negative than χ_{BC}.[35,44−48] Different hydrogen-bonding-interaction strengths lead to the formation of a variety of composition-dependent microphase separations.

In addition, the self-assembly structure of amphiphilic block copolymers in thermosets have been used to prepare ordered and disordered nanostructures.[49−52] Recently, ordered mesoporous materials, such as phenolic resin or carbon with a high surface area, large pore volume, and mechanical stability, have received much attention for their potential applications in adsorption, separation, catalysis, photonics, and drug delivery. As a result, the formation of nanostructures in the blends of phenolic resins has been widely reported.[53−55] Phenolic resin can be divided into two classes: resol- and novolac-based materials. The resol-based nanostructures are generally obtained by in situ phenolic cross-linking in multicomponent mixtures of phenol, formaldehyde, water and block copolymers. The nanostructures are strongly affected by competitive kinetic effects, such as the evaporation of solvent, the self-assembly of block copolymers, and the cross-linking and vitrification of the resols.[56−58] Another class of phenolic resins can be prepared through the curing of novolac resins; for example, Ikkala and Ruokolainen et al. prepared the mesoporous phenolic resins (Scheme 1) from templates by PI-*b*-P2VP and PS-*b*-P4VP diblock copolymers with hexamethylenetetramine (HMTA) as the curing agent.[39,40,59] Zheng et al. reported the formation of nanostructures in phenolic thermosets resulting from the novolac and PS-*b*-PEO diblock copolymer cured with HMTA. The use of novolac resins instead of resols can allow investigation of the morphological evolutions before and after the curing reaction.[60] In all of the above studies, the phenolic resin is miscible with P4VP, P2VP, and PEO through hydrogen-bonding interactions, but it is immiscible with PS or PI, which could be classified as first case where C is only miscible with B, but is immiscible with A.

In this study, the PEO-*b*-PCL diblock copolymers or PCL-*b*-PEO-*b*-PCL triblock copolymer consists of two immiscible crystallizable blocks in which the PEO and PCL blocks are both miscible with phenolic resin from hydrogen-bonding interactions. This represents an A-*b*-B/C blend system as in the second case, where C is miscible with both A and B blocks. However, the hydrogen bonding between PEO and the phenolic resin was significantly stronger than that between PCL and the phenolic resin.[61] Selective hydrogen bonding between the phenolic/PEO pair at relatively lower phenolic contents and the coexistence of two competitive hydrogen-bonding interactions between phenolic/PEO and phenolic/PCL pairs at relative higher phenolic contents have been observed in this blend.[61] This effect leads to the formation of a variety of composition-dependent nanostructures, including disorder, gyroid and short-cylinder structures. The phase behaviors and competing interactions of the mesostructures were investigated by differential scanning calorimetry (DSC), Fourier-transform infrared (FT-IR) spectroscopy, small-angle X-ray scattering (SAXS), and transmission electron microscopy (TEM). This work demonstrates for the first time the preparation of a mesoporous phenolic resin through competitive hydrogen bonding with double-crystalline diblock copolymer/homopolymer blends where phenolic is miscible with both block segments. An interesting closed-loop mesoporous structure exists in the phase diagram of the mesoporous phenolic

Table 1. Characterization of PCL-*b*-PEO-*b*-PCL Triblock Copolymer and PEO-*b*-PCL Diblock Copolymers Used in This Study

sample	abbreviation	NMR M_n	PDI
$CL_{35}EO_{455}CL_{35}$	EC1	28 000	1.05
$EO_{114}CL_{84}$	EC2	15 000	1.31
$EO_{114}CL_{130}$	EC3	20 000	1.29
$EO_{114}CL_{168}$	EC4	25 000	1.31

resin templated by PEO-*b*-PCL block copolymers, which is similar to ternary polymer blends when all three binary pairs (B−A, B−C, and A−C) are individually miscible. A closed-loop immiscibility phase diagram has been observed due to the so-called "$\Delta\chi$" and "ΔK" effects in a hydrogen-bonded ternary polymer system.[62−65]

EXPERIMENTAL SECTION

Materials. Monomethoxy-poly(ethylene glycol) with a molecular weight of 5000 (MPEG-5K) and poly(ethylene oxide) with a molecular weight of 20 000 (PEO-20K) were obtained from Fluka and dried by azeotropic distillation with dry toluene. ε-Caprolactone (ε-CL, Acros) was purified by vacuum distillation over CaH_2. The distillation fraction collected at 96−98 °C (5 mm-Hg) was used in all polymerization reactions. Stannous(II) octoate [$Sn(Oct)_2$, Sigma Corp.] was used as received. Methylene chloride was dried over CaH_2 prior to use. The phenolic was synthesized with sulfuric acid in a condensation reaction, which produced average molecular weights (M_n = 500) that are described in previous studies.[66−68] Diblock and triblock copolymers were readily prepared through the ring-opening polymerization of ε-CL, mPEG-5K, and PEO-20K in the presence of $Sn(Oct)_2$ as the catalyst.[69] The reaction mixtures were prepared by introducing a desired volume of ε-caprolactone monomer into a silanized flask containing a preweighed amount of mPEG-5K and PEO-20K under a nitrogen atmosphere. One drop of $Sn(Oct)_2$ was added, and the flask was connected to a vacuum line, evacuated, sealed off and heated to 130 °C. After 24 h, the resulting block copolymers were dissolved in methylene chloride and precipitated in an excess of cold *n*-hexane. The polymers were dried at 40 °C under vacuum. The characterizations of the triblock copolymer and diblock copolymers used in this study are summarized in Table 1. The PCL-*b*-PEO-*b*-PCL triblock copolymer was synthesized to increase the PEO weight fraction in the block copolymer (>50 wt % PEO).

Synthesis of Mesoporous Phenolic Resins and Carbon. Phenolic resin, HMTA, and PEO-*b*-PCL were dissolved in THF until the solutions were homogeneous. THF was slowly evaporated at room temperature, and the samples were subsequently vacuum-dried at 30 °C for 1 d. Curing of the samples was performed using the following temperature profile: 100 °C for 2 h, 150 °C for 2 h, and 190 °C for 2 h. Pyrolysis of the cross-linked samples was performed by slowly heating the samples from room temperature to 330 °C at a rate of 1 °C/min in the absence of a protective gas atmosphere (Scheme 1). Mesoporous carbons were prepared using an evaporation induced self-assembly (EISA) strategy with PEO-*b*-PCL as the template, THF as the solvent, and phenolic resin as the carbon source. During a typical synthesis, pyrolysis of the cross-linked samples was carried out in a tubular furnace under N_2 at 800 °C for 3 h at a heating rate of 5 °C/min.

Characterizations. ^{1}H spectra were recorded at room temperature on a Bruker AM 500 (500 MHz) spectrometer using the residual proton resonance of the deuterated solvent as the internal standard and $CDCl_3$ as the solvent. Molecular weights and molecular weight distributions were determined by gel permeation chromatography (GPC) using a Waters 510 HPLC equipped with a 410 Differential Refractometer and three Ultrastyragel columns (100, 500, and 10^3 Å) connected in series; DMF was the eluent at a flow rate of 1.0 mL/min. Thermal analysis was performed using a Q-20 differential scanning calorimeter (DSC) from TA Instruments. The measurement was operated at a heating rate of 20 °C and a cooling rate of 5 °C/min from +150 to −90 °C in N_2; the sample weighted between 5 and 10 mg. FTIR spectra of the samples were recorded using the conventional KBr disk method. The spectra were recorded using a Bruker Tensor 27 FTIR spectrophotometer. SAXS measurements were taken on a Nanostar U small-angle X-ray scattering system (Bruker, Germany) using Cu Kα radiation (40 kV, 35 mA). The *d*-spacing values were calculated using the formula $d = 2\pi/q$. Nitrogen sorption isotherms were measured at 77 K with an ASAP 2020 analyzer. Prior to taking the measurements, the samples were degassed under vacuum at 200 °C for at least 6 h. The Brunauer−Emmett−Teller (BET) method was utilized to calculate the specific surface areas. Using the Broekoff−de Boer (BdB) sphere model, the pore volumes and pore size distributions were derived from the adsorption branches of isotherms, and the total pore volumes were estimated from the adsorbed amount at relative pressure (P/P_0 of 0.995). The calibration curve was obtained by using silica−alumina (part no. 004−16821−00) as a reference material and nitrogen as an adsorption gas. TEM experiments were conducted on a JEOL 3010 microscope (Japan) operated at 200 kV. All the sample preparation for TEM characterizations were through solution casting and without thermally annealing.

RESULTS AND DISCUSSION

Phenolic Resin/Block Copolymer Analyses. *Thermal Analyses.* We have reported that phenolic is totally miscible with PEO and PCL in the amorphous phase due to the interassociation hydrogen bonding between the hydroxyl group of the phenolic and either the carbonyl group of the PCL or the ether group of the PEO. In general, DSC analysis is a convenient method of determining the miscibility of polymer blends. The glass-transition temperature (T_g) of the pure polymers used in this study—phenolic, PEO, and PCL—are +66, −60, and −60 °C, respectively. Figure 1 shows the conventional second-run DSC thermograms of various compositions of phenolic/EC (EC means PEO-*b*-PCL here) blends (not cured with HMTA) obtained at a heating rate of 20 °C/min. The melting temperatures of both the PEO and PCL blocks were depressed with increasing phenolic resin content for all four blend systems.[70−74] The reduction in the melting temperature results from morphological effects and thermodynamic consequences of hydrogen-bonding interactions with the phenolic resins. Table 2 summarizes the thermal properties of phenolic/EC blends based on DSC analyses.

Because the T_gs of PEO and PCL are very similar, the miscibility between PEO and PCL cannot be determined using one or two T_gs. Guo et al. have reported that two separated crystalline microdomains exist in these diblock copolymers that are composed of PEO and PCL blocks.[46] The two T_gs of the PEO and PCL blocks shifted toward higher values with 20−60 wt % phenolic resins. The changes in the T_g values arise from the phenolic−PEO (higher T_g) and the phenolic−PCL (lower T_g) phases because the interassociation equilibrium constant between the phenolic hydroxyl group and the PEO ether group is greater than the interassociation equilibrium constant between the hydroxyl group of phenolic and the carbonyl group of PCL.[61] The T_g of the PCL block shifts toward a higher value with increasing phenolic content, whereas the T_g of the PEO block did not increase with phenolic content because the T_g is also dependent on the crystallinity of the PEO block. In general, the T_g of the amorphous PEO phase will increase with increasing phenolic/copolymer composition, but the presence of PEO

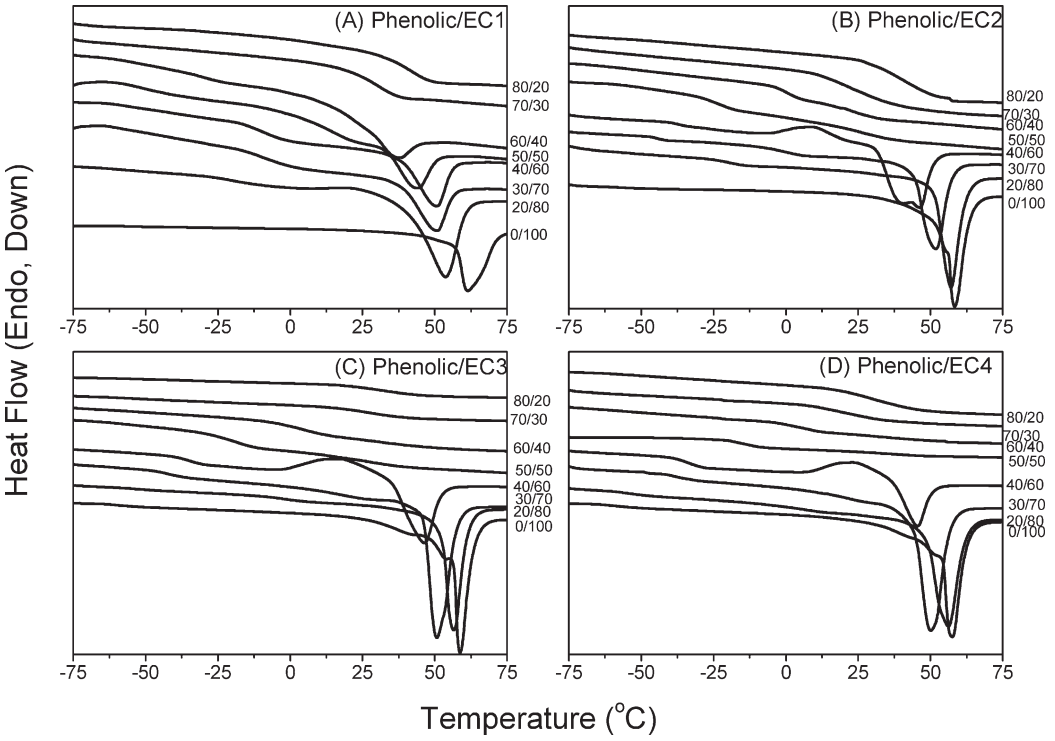

Figure 1. DSC thermograms of phenolic/EC blends, having different compositions for (a) phenolic/EC1, (b) phenolic/EC2, (c) phenolic/EC3, and (d) phenolic/EC.

crystals in this miscible blend (lower phenolic/copolymer ratio, ie. 20/80 or 30/70) is able to act as physical cross-linking points to hinder the molecular mobility of the amorphous phase. Therefore, the T_g of the PEO phase always goes through a minimum value at phenolic/copolymer = 60/40 because this composition exhibits the lowest crystallinity. The phenolic/EC blends exhibit only one T_g when the phenolic content is greater than 70 wt %, which suggests that these blends become miscible.

The miscibility windows also can be characterized by using SAXS analyses when crystalline component-containing blends as shown in Figure S1(a) (Supporting Information). Clearly, the phenolic/EC2 = 80/20 shows the disorder morphology, indicating that this blend is miscible. When phenolic content is below 60 wt %, the phase-separation was occurred, which is consistent with DSC analyses. Eventually, phenolic acts like a common solvent between PEO and PCL and induces the blends to become totally miscible (disordered structure). This behavior is similar to that of the phenolic/PEO/PCL[61] or PVPh/PEMA/PMMA[63] ternary blends, which become totally miscible at a phenolic resin and PVPh content greater than 65 wt %, respectively. More importantly, we are interested in investigating the morphological transformation and self-organized mesoporous structure in this immiscible block copolymer/phenolic-blend composition by TEM and SAXS, the results of which are discussed in later sections.

FT-IR Analyses. As mentioned in the discussion of the DSC results, the hydrogen-bonding strength in the phenolic/PEO system is greater than that of the phenolic/PCL blend system. When the phenolic content is increased further, phenolic becomes available to interact with both PEO and PCL through hydrogen bonding. At 70 wt % phenolic, the blends become miscible and phenolic acts as a common solvent in this blend system. As a result, we used FTIR spectroscopy to provide evidence of this common solvent effect.

Several regions within the FTIR spectra of the phenolic/EC blends are influenced by the hydrogen-bonding interactions. For convenience, only selected infrared spectra of phenolic/EC1 blends are employed in this study. The hydroxyl stretches of various phenolic/EC1 blends and those of pure phenolic cast from THF solution are shown in Figure 2. Pure phenolic shows two unresolved bands in the hydroxyl stretching region: one corresponds to the free hydroxyl at 3525 cm^{-1}, and the other broad band centered at 3350 cm^{-1} corresponds to the absorption of a hydrogen-bonded hydroxyl group (self-association), as shown in Figure 2a. The intensity of the band from the free hydroxyl group gradually decreases with increasing EC1 content in this blend system, as would be expected. In addition, Figure 2a demonstrates that the hydroxyl band shifts to a lower wavenumber when the blend is rich in EC1 (lower phenolic content), which implies that the phenolic hydroxyl preferably interacts with the PEO ether. Therefore, it is reasonable to assign the band at 3225 cm^{-1} to the hydroxyl that is hydrogen-bonded with ether because a relatively smaller number of the hydroxyl groups tend to interact completely with the ether groups of the PEO block to form hydrogen bonds.

The peak frequency of the broad band shifts to higher wavenumbers with increasing phenolic content. This shift reflects a new distribution of the formation of hydrogen bonds resulting from the competition between the hydroxyl−hydroxyl group within the pure phenolic and the hydroxyl−carbonyl group between phenolic and PCL (3430 cm^{-1}). Moskala et al. have used the frequency difference between the hydrogen-bonded hydroxyl absorption and the free absorption ($\Delta\upsilon$) to roughly estimate the average hydrogen-bonding strength.[75] In this respect, hydrogen-bonding interactions between phenolic hydroxyl and the PEO ether ($\Delta\upsilon$ = 300 cm^{-1}) are stronger than those between phenolic hydroxyl and the PCL carbonyl

Table 2. Thermal Properties of Phenolic/EC blends

	T_g (°C)			
phenolic/EC			T_m(°C)	ΔH_f (J/g)
pure phenolic	64			
phenolic/EC1				
80/20	30			
70/30	26			
60/40	−30	22	37	4.6
50/50	−39	14	43	8.5
40/60	−40	−8	50	9.4
30/70	−50	−9	51	12.0
20/80	−54	21	54	38.8
0/100	−60		61	126.9
phenolic/EC2				
80/20	42			
70/30	22			
60/40	0	20		
50/50	−26	16		
40/60	−37	−24	46	28.6
30/70	−44	1	51	32.6
20/80	−50	19	57	43.6
0/100	−60		58	95.5
phenolic/EC3				
80/20	31			
70/30	28			
60/40	3	31		
50/50	−18	28		
40/60	−35	−21	46	18.7
30/70	−42	19	51	28.1
20/80	−53	−3	57	43.1
0/100	−60		59	156.0
phenolic/EC4				
80/20	28			
70/30	23			
60/40	6	26		
50/50	−18	36		
40/60	−32	−13	46	12.0
30/70	−39	21	50	49.2
20/80	−54	6	56	57.9
0/100	−60		58	119.0

($\Delta\upsilon = 95$ cm^{-1}). These results are consistent with the prediction from the Painter−Coleman association model (PCAM).[76,77] According to the PCAM, the interassociation equilibrium constant of the phenolic/PEO blend ($K_A = 264$) is greater than that of the phenolic/PCL blend ($K_A = 116$), which implies that the formation of hydrogen bonds between phenolic and PEO predominates over that between phenolic and PCL in these phenolic/EC blends.[61]

The carbonyl groups of PCL blocks are sensitive to hydrogen-bonding interactions. The peaks at 1735 and 1705 cm^{-1} correspond to the free carbonyl and hydrogen-bonded carbonyl, respectively. Figure 2b presents FTIR spectra of the carbonyl stretching region, which ranges from 1680 to 1780 cm^{-1}, of pure EC1 and phenolic/EC1 blends. The hydrogen-bonded carbonyl band of PCL at 1705 cm^{-1} starts to appear in the blends that contain a phenolic content of 50 wt % or greater, which indicates that the phenolic hydroxyl starts to interact with the PCL carbonyl. As expected, a higher content of phenolic units results in a higher number of hydrogen-bonded carbonyl groups.

The band at 1100 cm^{-1} also can be used to analyze the hydrogen-bonding interactions between the hydroxyl group of phenolic and the ether group of PEO. Figure 2c shows the scale-expanded infrared spectra in the range 1050−1140 cm^{-1} for phenolic/EC1 blends. Pure EC1 has a characteristic band at 1112 cm^{-1} that corresponds to the C−O−C ether absorption of the PEO block. Upon the formation of hydrogen bonds between phenolic and PEO, this band shifts to 1100 cm^{-1}; this effect is attributed to hydrogen-bonded ether at a phenolic resin content of 20 wt % or greater.[63]

Figure 3 shows the FTIR spectra of the phenolic/PEO-*b*-PCL blends that contain a fixed phenolic content (50 and 60 wt %) as the weight fraction of PEO in the block copolymers is varied. The hydrogen-bonded fraction of the carbonyl group clearly decreases with an increasing relative PEO/PCL ratio in the block copolymers. In other words, the PCL carbonyls compete with the ether oxygen atoms of PEO to form hydrogen bonds with the hydroxyl groups of the phenolic resin. We also investigated the IR spectra of phenolic/EC2 blend with variable temperature as shown in Figure S2 (Supporting Information). Clearly, only the hydrogen bonding interacting carbonyl group was decreased at high temperature, the absorption band of the crystalline carbonyl group at 1724 cm^{-1} did not change due to the disappearance of crystalline PCL after blending. The Gaussian function has been used to fit the carbonyl stretching bands of PCL at 1735 and 1705 cm^{-1} that correspond to their respective free and hydrogen-bonded groups. The fraction of the hydrogen-bonded carbonyl group can be calculated using an appropriate absorptivity ratio ($a_R = a_{HB}/a_F = 1.5$), as has been intensively discussed in our previous study.[70] The results of the curve fittings are summarized in Figure 4. The experimental results show the fraction of hydrogen-bonded carbonyl in PCL increased with increasing phenolic resin content, which is similar to the prediction made using the PCAM. Table 3 lists all of the parameters required by the PCAM to estimate thermodynamic properties for the blends in this study. In addition, the hydrogen-bonded fraction of the carbonyl group decreases with an increasing PEO/PCL relative weight ratio in the block copolymers. These results are also similar to the PCAM prediction results. The PCAM is able to predict the hydrogen-bonded fraction of the carbonyl group at higher phenolic contents, as shown in Figure 4, because these composites are miscible. The deviation of the PCL hydrogen-bonded carbonyl group at relatively low phenolic contents changed from a positive to a negative deviation as the composition of PEO in the block copolymers was increased. The main reason for such a change in deviation is that the interassociation equilibrium constant of phenolic/PEO is greater than that of phenolic/PCL; thus, the PCL tends to be excluded from the phenolic/PEO phase. The microphase separation of the PCL block decreases the intermolecular hydrogen-bonding interaction between phenolic and PCL; as a result, the experimental results for a hydrogen-bonded carbonyl group are lower than those predicted for an increase of the PEO weight fraction. Here, we need to emphasize that the interassociation equilibrium constant between the phenolic hydroxyl group and the PEO ether group is still an open question because the ether-stretching mode near 1100−1200 cm^{-1} is a highly coupled mode that is conformationally sensitive and cannot be readily deconvoluted

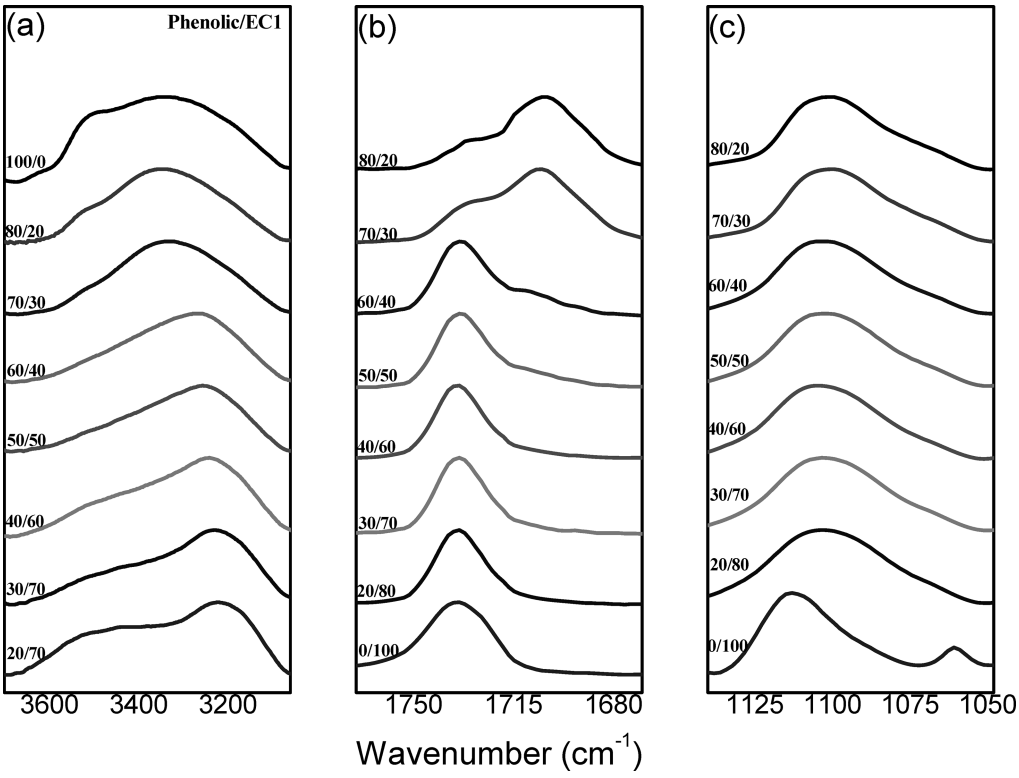

Figure 2. FT-IR spectra recorded at room temperature displaying the (a) hydroxyl stretching, (b) carbonyl, and (c) ether region.

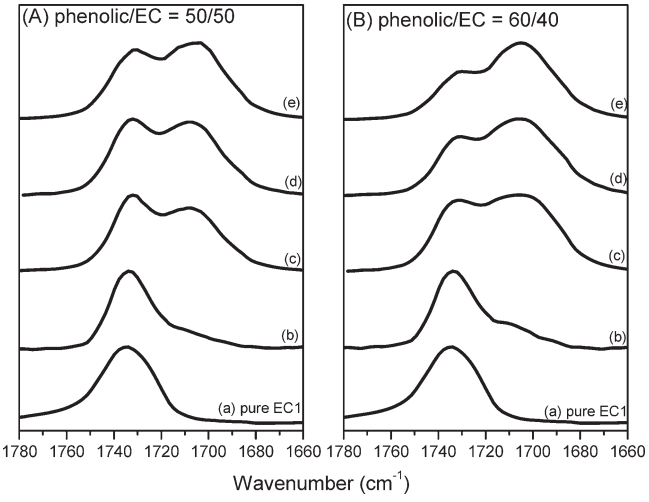

Figure 3. FT-IR spectra recorded at room temperature displaying the carbonyl region of phenolic/EC blends fixing phenolic contents (50 and 60 wt %) for (a) pure EC1, (b) phenolic/EC1, (c) phenolic/EC2, (d) phenolic/EC3, and (e) phenolic/EC4.

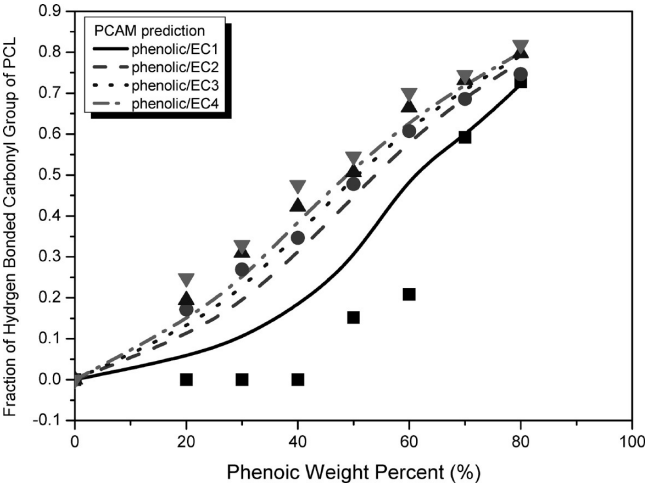

Figure 4. Experimental and prediction data for $f_{HB}^{C=O}$ of phenolic/EC blends with different phenolic weight percent for (■) phenolic/EC1, (●) phenolic/EC2, (▲) phenolic/EC3, and (▼) phenolic/EC4.

into two peaks with areas that correspond to the free and the hydrogen-bonded ether absorptions.[77] The K_A value is determined indirectly from a least-squares fitting procedure of the experimental fraction of the hydrogen-bonded carbonyl group in the ternary polymer blend.[61] It may also exhibit a deviation because of different miscibility behaviors with various phenolic compositions used in this study.

Mesoporous Phenolic Resin Analyses. *Thermal Analysis Prior to Pyrolysis of Block Copolymers.* We first investigated the thermal behavior of the phenolic/EC blends prepared with HMTA as a curing agent prior to pyrolysis. Although the microphase separation existed in the cured blends of phenolic thermosets with the blocks, it could result from reaction-induced demixing from homogeneous mixtures.[78] We first examine the morphologies of the uncured ternary blends of novolac, block copolymer and HMTA by using SAXS as shown in Figure S1(b) (Supporting Information). The similar SAXS pattern was observed compared with phenolic/EC blend without HMTA. In general, DSC analysis is a convenient method of determining

dx.doi.org/10.1021/ma2010734 |*Macromolecules* 2011, 44, 9295–9309

Table 3. Summary of the Self-Association and Inter-Association Equilibrium Constants and Thermodynamic Parameter of Phenolic/EC Blends at Room Temperature

				self-association equilibrium constant		interassociation equilibrium constant	
polymer	molar volume (mL/mol)	molecular weight (g/mol)	solubility parameter $(cal/mL)^{0.5}$	K_2	K_B	K_A	K_C
phenolic	84.0	105.0	12.05	23.3	52.3		
PEO	38.1	44.1	9.40			264.7	
PCL	102.1	114.1	9.21				116.8

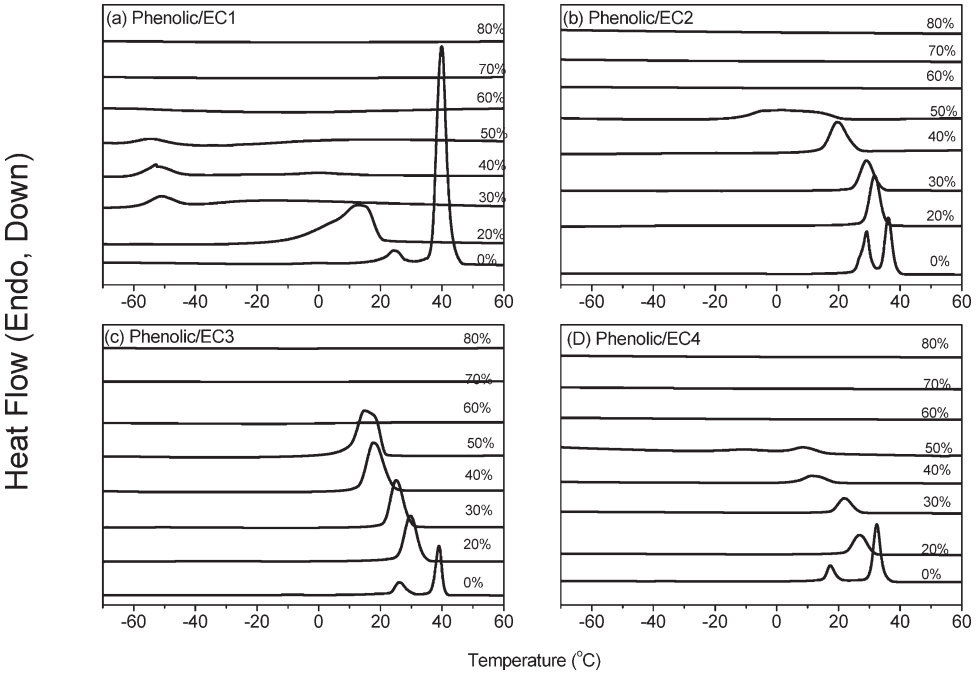

Figure 5. DSC cooling curves of phenolic/EC blends after curing HMTA for (a) phenolic/EC1, (b) phenolic/EC2, (c) phenolic/EC3, and (d) phenolic/EC4 having different phenolic resin contents with a constant cooling rate of 5 °C/min.

crystallization behavior in polymer blends. Figure 5 shows the DSC traces of pure EC block copolymers and phenolic/EC blends cured with HMTA recorded during the cooling scan at a cooling rate of 5 °C/min. The peak temperature of the crystallization exotherm is defined as the freezing temperature (T_f); a higher T_f corresponds to a faster crystallization rate. Previous works have reported that the T_f is associated with the nonisothermal crystallization under a fixed cooling rate and displays a distinct correlation with the microdomain structure.[79−84]

All of the EC block copolymers exhibited two crystallization peaks. The higher and lower crystallization peaks correspond to the PEO block and the PCL block, respectively. The crystallization ability of the PEO block is restricted by the PCL block, which is covalently coupled to the other end of the PEO block. These results indicate that two separated crystalline microdomains exist in the diblock copolymers that comprise the PEO and PCL blocks. As expected, the crystallization peaks shift to lower T_f values with increasing phenolic resin content. These results are consistent with Figure 1, in which the melting temperatures were depressed with increasing phenolic resin content for all four blend systems. More interestingly, in the phenolic/EC1 crosslinked sample, a relatively lower T_f at approximately −53 °C for samples with 30, 40, and 50 wt % phenolic content was observed. These lower T_f values are not present in the PEO or PCL homopolymers, which appear at much larger undercooling. Chen et al.[79,80] reported that the degree of supercooling ($\Delta T = T_m^0 - T_f$, T_m^0 = 75 °C)[74] required to initiate crystallization in the lamellar microdomains (ΔT = 50 °C) is comparable to that associated with the PCL homopolymer (ΔT = 42 °C); exceedingly large undercoolings are required for crystallizations in the cylindrical microdomains (T_f = −50 °C, ΔT = 125 °C).[84] As a result, the exotherm at a lower T_f (−53 °C) may originate from the PCL block in a 2D cylindrical confinement (ΔT = 124 °C) because the lowest T_f of the PEO block in a 3D sphere confinement was −30 °C.[65]

The crystallization kinetics exhibited distinct transitions at the compositions that correspond to the morphological transformation, which demonstrates the feasibility of exploring the microdomain pattern by manipulating the crystallization kinetics of the block chains. As a result of the special confinement effect of the double-crystalline amphiphilic PEO-*b*-PCL diblock copolymer, we can utilize a more convenient method that uses DSC to characterize the morphology of mesoporous nanostructures in a PEO-*b*-PCL crystalline−crystalline diblock copolymer. This method will not work, however, in a crystalline−amorphous diblock copolymer, such as PEO-*b*-PS,[55] or in an amorphous−amorphous diblock copolymer, such as PI-*b*-P4VP or PS-*b*-P4VP.[59]

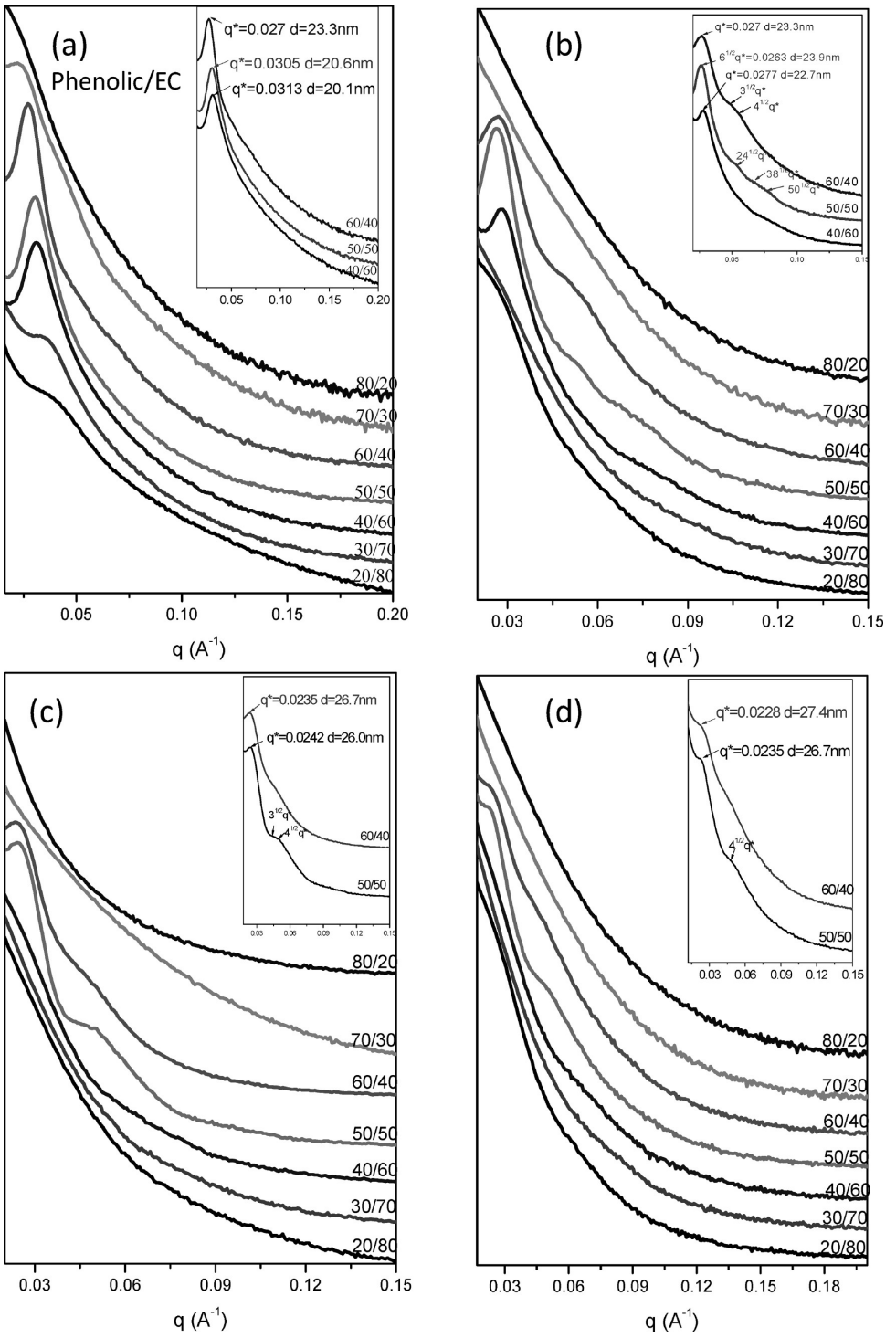

Figure 6. Profiles of Lorentz-corrected SAXS intensity of mesoporous phenolic resin from templated by (a) EC1, (b) EC2, (c) EC3, and (d) EC4 block copolymers.

SAXS, TEM, and BET Analyses of Mesoporous Phenolic Resin. SAXS profiles of mesoporous phenolic resins templated by EC block copolymers were taken at room temperature to confirm the self-organized mesoporous morphologies at room temperature, as shown in Figure 6. These figures suggest that the phenolic contents influence the formation of the mesostructure. We also investigated the self-assembly structures of phenolic resins templated by EC block copolymers prior to pyrolysis of block copolymers as shown in Figure S3 (Supporting Information). Clearly, the microphase separation was observed, which is similar to the mesoporous phenolic resins in this study. In Figure 6a, which represents a mesoporous phenolic resin templated by EC1 triblock copolymer, broad peaks corresponding to the short-range-order mesoporous phenolic resin are observed at relatively lower phenolic contents (<30 wt %). These results are consistent with the TEM image in Figure 7a. The blends with 40, 50, and

dx.doi.org/10.1021/ma2010734 |*Macromolecules* 2011, 44, 9295–9309

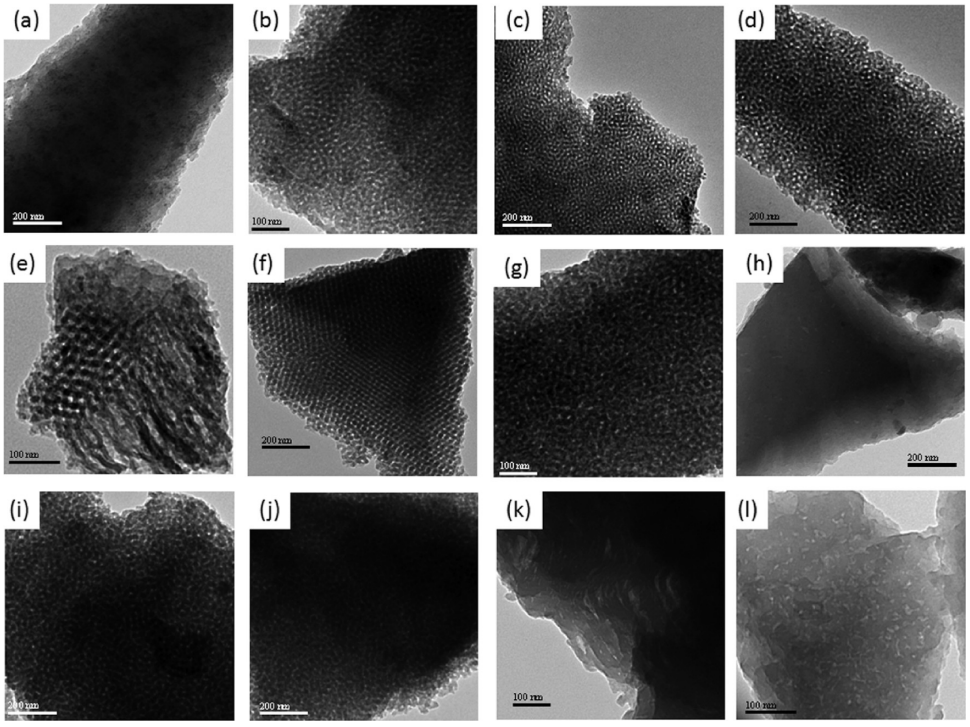

Figure 7. TEM images of mesoporous phenolic from phenolic/EC1 for (a) 30/70, (b) 40/60, (c) 50/50, and (d) 60/40, phenolic/EC2 for (e) 40/60, (f) 50/50, (g) 60/40, and (h) 70/30, phenolic/EC3 for (i) 50/50 and (j) 60/40, and phenolic/EC4 for (k) 50/50 and (l) 60/40 blends.

60 wt % phenolic contents give only one peak that correspond to short-range-order mesoporous phenolic resin. These values are characteristic of a disordered spherical structure, which was further confirmed by TEM as shown in Figure 7, parts b−d, and Figure S4 (Supporting Information) by microtoming. They show only weak and broad peaks at phenolic contents greater than 70 wt %, which indicates near-disorder and short−long order morphology. In 70 wt % phenolic blends, the blends become miscible and phenolic acts as a common solvent in this blend system due to the hydrogen bonding of phenolic with both the PEO and PCL block segments. In addition, according to the positions of the first-order scattering peaks, the average spacing between the neighboring microdomains is 20.1, 20.6, and 23.3 nm for samples containing 40, 50, and 60 wt % phenolic, respectively, as shown in the inset of Figure 6a. This result indicates that the size of the mesoporous domains systemically increase with increasing phenolic content.

In Figure 6b, which represents mesoporous phenolic resin templated by the EC2 diblock copolymer, a remarkable mesophase transformation through disordered (20 and 30 wt %), short-range ordered (40 wt %), bicontinuous gyroid (50 wt %), short cylinder (60 wt %) and finally to disordered structures (70 and 80 wt %) was observed with increasing phenolic resin content. The short-range-order morphology was observed at 40 wt % phenolic based on only one scattering peak at $q^* = 0.27\ \mathrm{nm}^{-1}$ ($d = 23.2$ nm), which was consistent with the TEM image in Figure 7e. A complete mesoporous structure at a relatively lower phenolic content was not able to form due to insufficient phenolic resin. An ordered bicontinuous gyroid structure was observed at 50 wt % based on SAXS; the intensity maximum appears at $6^{1/2}q^* = 0.26\ \mathrm{nm}^{-1}$ ($d = 24.1$ nm). The order reflections at $24^{1/2}q^*$, $38^{1/2}q^*$ and $50^{1/2}q^*$ were observed, as shown in inset Figure 6b, and are characteristic of long-range order in a bicontinuous gyroid structure. These results were further confirmed by TEM images, as shown in Figure 7f. The maximum intensity appeared at approximately $q^* = 0.26\ \mathrm{nm}^{-1}$ ($d = 24.1$ nm) and higher-order reflections at $3^{1/2}q^*$ and $2q^*$ were exhibited at 60 wt % phenolic content, as shown in the inset in Figure 6b. These values were characteristic of a short cylindrical structure, which was further confirmed by TEM because the volume fraction of the phenolic resin raised the outer domain, as shown in Figure 7g. However, it exhibited a disordered structure at 70 wt % phenolic, as determined by SAXS, based on the appearance of broad peaks that indicated the absence of a long-range ordered structure; this result was further confirmed by TEM, as shown in Figure 7h. This result also agreed with the DSC and FTIR analyses. The phenolic hydroxyl was able to form hydrogen bonds with both PEO and PCL according to FTIR spectroscopy (Figure 3). A completely miscible blend, as determined by DSC analysis, was due to only one single T_g in Figure 1 when the phenolic content was 70 wt %. SAXS profiles of mesoporous phenolic resin templated by EC3 and EC4 block copolymers are shown in Figure 6, parts c and d. Clearly, the long-range-order structure was decreased when the blends were templated by EC3 and EC4 diblock copolymers instead of EC1 and EC2 block copolymers. This result indicates that due to the increase in the relative PCL/PEO ratio in the block copolymers, the PCL carbonyl competes with the ether oxygen of PEO to form a hydrogen bond with the hydroxyl group of the phenolic resin, as shown in Figure 4. The short cylinder was found at 50 and 60 wt % phenolic templated by EC3 diblock copolymer, as demonstrated in Figure 6c; this result was further confirmed by TEM, as shown in Figure 7, parts i and j. The near-weak and broad peaks at 50 and 60 wt % phenolic contents templated by EC4 diblock copolymer, as shown in Figure 6d, indicate a near short cylinder and homogeneous morphology, which was further confirmed in Figure 7, parts k and l, by TEM.

dx.doi.org/10.1021/ma2010734 |*Macromolecules* 2011, 44, 9295–9309

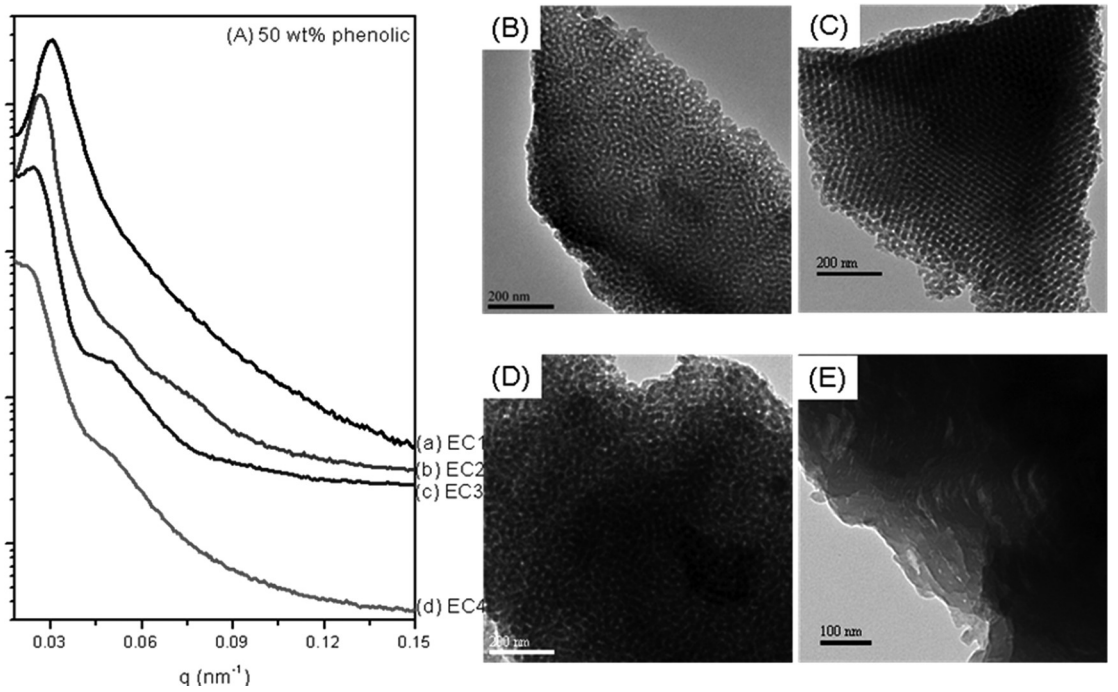

Figure 8. Summary of SAXS analyses (A) and TEM images of mesoporous phenolic resin containing fixing 50 wt % phenolic resin contents with different templated block copolymers for (B) EC1, (C) EC2, (D) EC3, and (E) EC4.

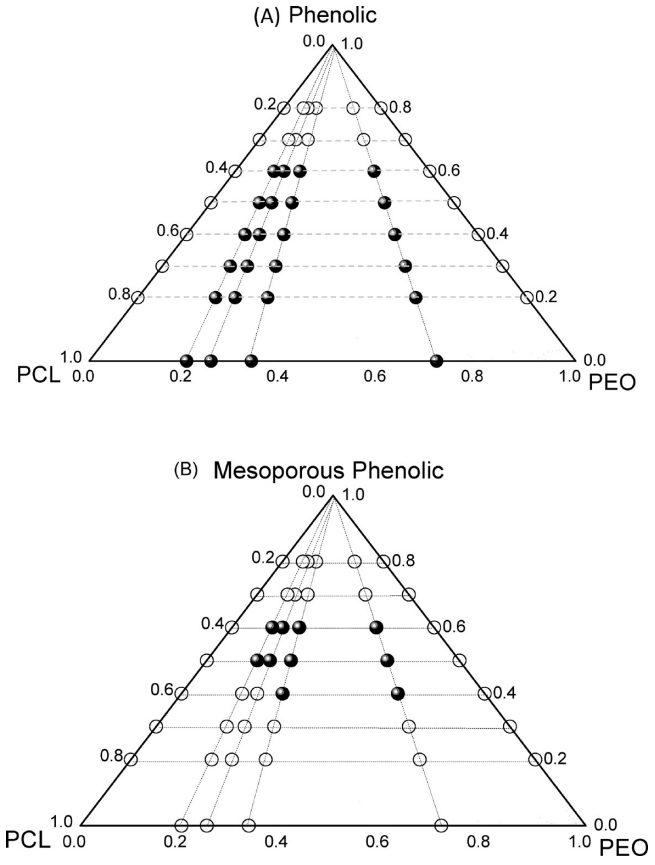

Figure 9. Phase diagram of (A) phenolic/EC blends, the open circle represent miscible disorder structure, the full circles represent microphase separation structure and (B) mesoporous phenolic resin from template by EC block copolymers, the open circles represent disorder structure and the full circles represent regular mesoporous structure.

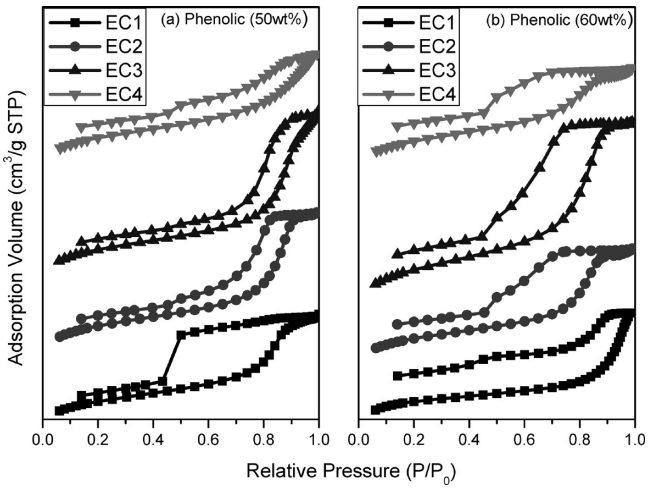

Figure 10. N_2 adsorption−desorption isotherms of mesoporous phenolic resins templated by different EC block copolymers with different phenolic weight percents (a) 50 wt %, and (b) 60 wt %.

Figure 8 summarizes the SAXS patterns and TEM images of the mesoporous phenolic resin templated by different EC block copolymers containing a fixed phenolic content (50 wt %) by changing the weight fraction of PCL in the block copolymers. According to the positions of the first-order scattering peaks, the average spacing between the neighboring microdomains was increased and the long-range-order structure decreased with increasing relative PCL/PEO ratios in the block copolymers. These effects occurred because the hydrogen-bonded fraction of the carbonyl group increased with the increased PCL/PEO ratios, as shown in Figure 4. In other words, the phenolic hydroxyl groups interact with the PCL carbonyl, which decreases the long-range-order structure to a disordered structure at relatively higher

dx.doi.org/10.1021/ma2010734 |*Macromolecules* 2011, 44, 9295–9309

phenolic contents. This interaction would increase the average size of long-period structures in the mesoporous phenolic resin. Therefore, the key point for preparing mesoporous phenolic templated by EC block copolymers is that the phenolic hydroxyl should have hydrogen-bonding interactions with the PCL carbonyl; however, the fraction of hydrogen-bonding PCL carbonyl should not be high enough to become a miscible disorder system. As a result, the regular mesoporous phenolic resin templated by EC block copolymers is strongly dependent on the phenolic resin contents and the relative PEO/PCL ratios.

The phase diagram of phenolic/EC blends based on DSC analysis and that of mesoporous phenolic templated by EC block copolymers based on SAXS patterns and TEM images is summarized in Figure 9. The presence of phenolic is able to enhance the miscibility of immiscible block copolymers of PEO and PCL with more than 70 wt % phenolic, as shown in Figure 9A. This result is similar to previous studies by Pomposo et al. on the PVPh/PEMA/PMMA ternary hydrogen-bonded polymer blend showing that the PVPh is miscible with other components with more than 65 wt % of PVPh.[85] However, a closed-loop mesoporous phenolic resin templated by EC block copolymers exists, as shown in Figure 9B, which is similar to ternary polymer blends when all three binary pairs (B−A, B−C, and A−C) are individually miscible. A closed-loop immiscibility phase diagram has been observed due to the so-called "$\Delta\chi$" and "ΔK" effects in hydrogen-bonded ternary polymer systems, including PVPh/PVAc/PEO,[63] SAA/PMMA/PEO,[64] and PVPh/PMMA/PEO.[86] At lower phenolic contents (<30 wt % phenolic), the system contained insufficient phenolic resin to template EC block copolymer and form a disorder structure. At higher phenolic content (>70 wt % phenolic), a complete miscible disordered structure was found because the phenolic hydroxyl was able to form hydrogen bonds with both PEO and PCL, according to FTIR spectroscopy. As a result, the self-organized mesoporous phenolic resin was only found at 40−60 wt % phenolic content by an intriguing balance of the contents of phenolic, PEO, and PCL. In addition, the mesoporous structure was destroyed when the PCL/PEO ratio in the block copolymers was increased.

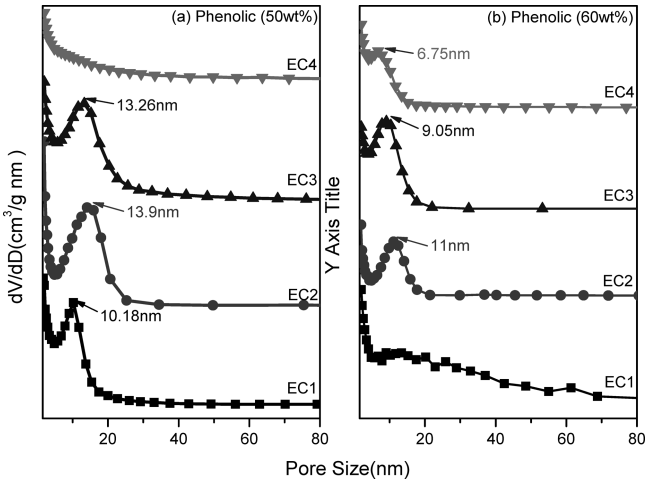

Figure 11. Pore size distribution curves of mesoporous phenolic resins templated by different EC block copolymers with different phenolic weight percents: (a) 50 wt % and (b) 60 wt %.

Nitrogen-sorption isotherms of mesoporous phenolic behaved like representative type-IV curves with a sharp capillary condensation step in the relative pressure range of 0.85 to 0.95, as shown in Figure 10. These data indicate the generation of mesopores with a large uniform size. The mesoporous phenolic samples templated by EC copolymers at 50 and 60 wt % phenolic contents exhibited a typical H_1-like hysteresis loop at P/P_0 = 0.4 to 0.9, which indicates a common mesoporous structure with large, branched, cylindrical pores. The H_1 hysteresis loop for these samples was characteristic of cylindrical mesopores. On the basis of the Harkins and Jura model,[87] the mean pore sizes measured from the adsorption branch were 10.2, 13.9, and 13.3 nm for mesoporous phenolic templated by EC1, EC2, and EC3 block copolymers, respectively. We did not, however, find the mean pore size templated by EC4 block copolymers at 50 wt % phenolic content, as shown in Figure 11a. Furthermore, the mean pore sizes measured from the adsorption branch were 11.0, 9.1, and 6.8 nm for mesoporous phenolic templated by EC2, EC3, and EC4 block copolymers, respectively. Because the mean pore size was strongly dependent on the molecular weight of the PEO segments and the PEO/PCL ratio of the block copolymers, we did not compare the results with the EC1 triblock copolymers.

The BET surface area, pore volume, and BJH pore size of the mesoporous phenolic materials are summarized in Table 4. The total BET surface area and the total pore volume decreased with increasing phenolic contents of the templated EC block copolymers; the pore size decreased with increasing PCL/PEO ratio in EC2, EC3, and EC4 diblock copolymers. For example, the total

Table 4. Textual Properties of the Mesoporousphenolic Resins and Carbon Products

sample	phenolic/EC	d (nm)[a]	pore size (nm)	S_{BET} (m^2/g)[b]	S_M (m^2/g)[b]	pore volume (cm^3/g)	micropore volume (cm^3/g)
phenolic/EC1	60/40	23.3	-	61	25	0.07	0.01
phenolic/EC1	50/50	20.6	10.2	386	158	0.40	0.07
phenolic/EC1	40/60	20.1	6.8	435	168	0.44	0.07
phenolic/EC2	60/40	23.3	11.0	68	22	0.07	0.01
phenolic/EC2	50/50	23.9	13.9	328	147	0.35	0.07
phenolic/EC2	40/60	22.7	15.6	403	202	0.42	0.09
phenolic/EC3	60/40	26.7	9.1	137	43	0.16	0.02
phenolic/EC3	50/50	26.0	13.3	391	203	0.43	0.09
phenolic/EC4	60/40	27.4	6.8	66	18	0.07	0.01
phenolic/EC4	50/50	26.7	-	193	92	0.17	0.04
carbon[c]	50/50	18.6	11.0	858	647	0.59	0.30

[a] The d-spacing values were calculated by the formula $d = 2\pi/q^*$. [b] S_{BET} and S_M are the total BET surface area and micropore surface area calculated from the t-plots, respectively. [c] Mesoporous carbon was synthesized from phenolic/EC2 = 50/50 pyrolyzed at 800 °C in N_2.

dx.doi.org/10.1021/ma2010734 |Macromolecules 2011, 44, 9295–9309

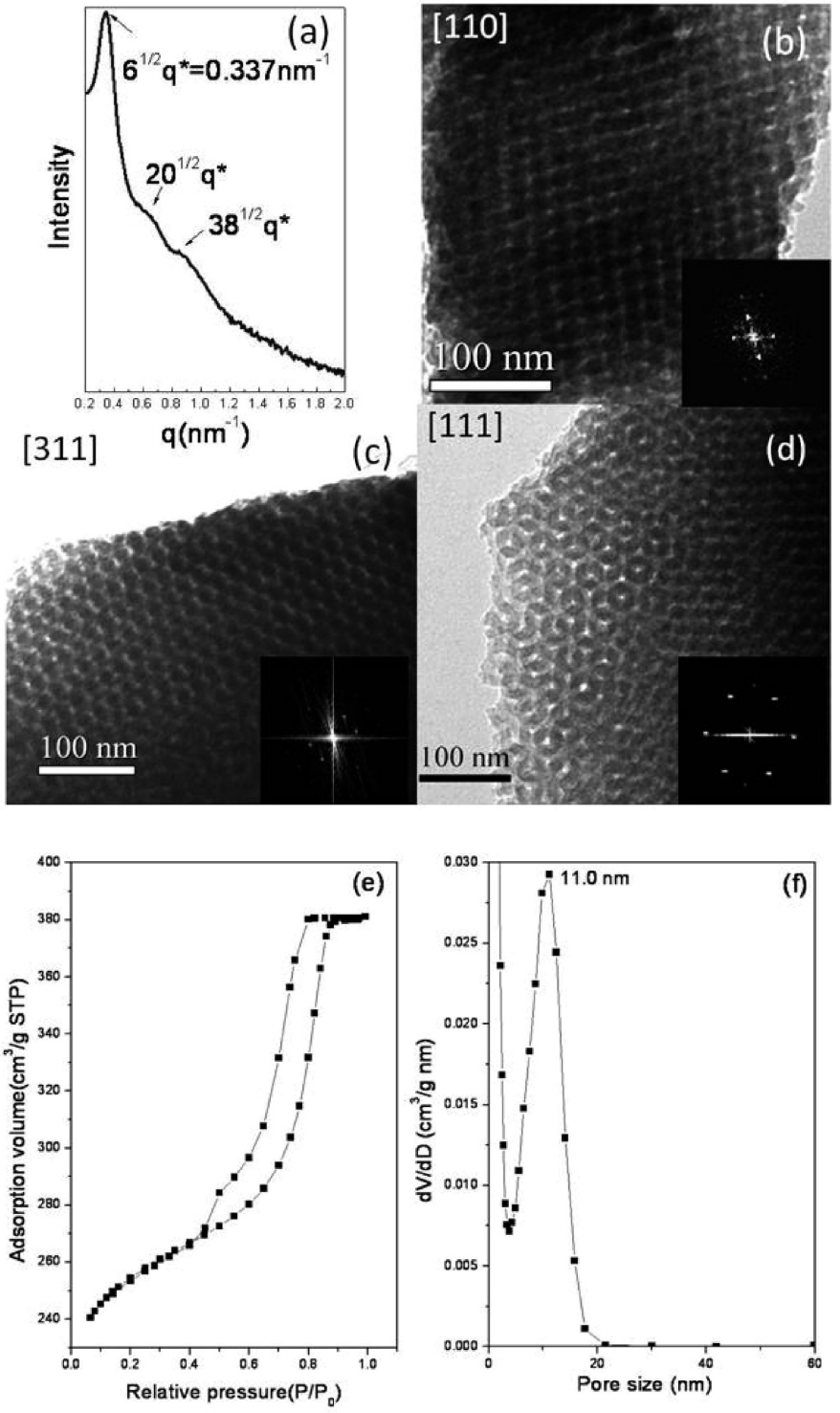

Figure 12. SAXS pattern (a), TEM images (b−d), N_2 adsorption−desorption isotherms (e), and pore size distribution curves (f) of mesoporous of gyroid mesoporous carbon pyrolyzed from mesoporous phenolic resin templated by EC2 block copolymer at 50 wt % phenolic resin content at 800 °C.

pore volume and total BET surface area of 50 wt % mesoporous phenolic templated by EC2 diblock copolymer were 0.35 and 328 m^2/g, respectively. These values were much larger than those of 60 wt % mesoporous templated by EC2 diblock copolymer, which confirms the presence of the distorted short-cylinder mesopores that were transferred from the cylindrical mesopores of the gyroid structure. To the best of our knowledge, this study is the first to fabricate a long-range order of bicontinuous gyroid-type mesoporous phenolic resin using an evaporation-induced self-assembly strategy. The mesoporous phenolic resin thin film, such as the mesoporous carbon discussed in the next section, can be obtained and applied in various fields.

Morphology of Mesoporous Carbon. Figure 12 displays the SAXS pattern, TEM images and BET analyses of gyroid mesoporous

carbon pyrolyzed from mesoporous phenolic resin (phenolic/EC2 = 50/50). Figure 12a presents the set of Bragg reflections with approximate relative q values of $6^{1/2}q^*$, $20^{1/2}q^*$, and $38^{1/2}q^*$, which correspond to a gyroid ($Ia\bar{3}d$) structure. This pattern is the same as that of gyroid phenolic resin, for which the d-spacing is calculated to be 23.6 nm (Table 4). Furthermore, the well-resolved SAXS pattern is retained, which indicates that the highly ordered mesostructure of the mesoporous carbon is thermally stable after calcination at 800 °C in N_2. The d-spacing is as large as 18.6 nm for the mesoporous carbon, which reflects a 21% shrinkage of the polymer framework. Parts b−d of Figure 12 show TEM images and corresponding Fourier diffractograms that indicate the mesoporous carbon has a high degree of periodicity over large domains. This result is viewed from the [110], [311], and [111] directions from the gyroid phenolic resin calcined at 800 °C under N_2.

Figure 12e shows the texture of the mesoporous carbon characterized by N_2 physisorption experiments and the corresponding N_2 adsorption−desorption isotherms and pore-size distributions. We observed that the gyroid carbon was also a typical mesoporous material. In Figure 12e, the gyroid carbon exhibited representative type-IV isotherms with H_1 hysteresis loops according to IUPAC classification.[88] These isotherms suggest that the uniform, large, cylindrical pores were retained. Furthermore, sharp steps occurred at relative pressures of 0.45 to 0.85 for this sample, which indicates a full filling of the uniform mesopores from the capillary forces. Compared with the gyroid mesoporous phenolic resin, the mean pore size measured from the adsorption branch decreased to 11.0 nm, as shown in Figure 12(f) and Table 4. The BET surface area and pore volume were 858 m^2/g and 0.59 cm^3/g, respectively. The BET surface area was much larger than that of the gyroid mesoporous phenolic resin due to the continuous removal of carbon, hydrogen, and oxygen from the mesoporous matrix during pyrolysis. The t-plot calculation revealed that the micropore surface area of the mesoporous carbon was 647 m^2/g, which is much larger than that of the mesoporous phenolic resin. This process was primarily responsible for introducing the micropores, which demonstrates that micropores are generated during the carbonization.

Because both blocks of PEO-*b*-PCL could interact with phenolic resin, the mesoporous phenolic resins or the mesoporous carbons templated by PEO-*b*-PCL could form a thicker wall in the mesoporous structures. The wall thickness of mesoporous materials is an important issue because thicker walls impart better thermal stability and mechanical properties.[89] The wall thickness of gyroid-type mesoporous phenolic resin and mesoporous carbon can be calculated using two equations of $w = a/2 - D$ and $a = \sqrt{6}d_{211}$ where w is the wall thickness, a is the unit-cell parameter, D is the pore diameter calculated from the adsorption branch of the isotherm using the BJH method, and d_{211} is the d-spacing calculated from the primary peak of SAXS.[90] On the basis of previously discussed equations, we obtained wall thicknesses of gyroid-type mesoporous phenolic resin and carbon of 15.4 and 11.8 nm, respectively. This study is the first report of the synthesis of thick walled gyroid-type mesoporous phenolic resin and carbon.

CONCLUSIONS

DSC, TEM, SAXS, and FT-IR techniques have been employed to perform a detailed investigation of the miscibility and hydrogen bonding interactions that result from the microphase separation of self-organized mesoporous phenolic resins through blends composed of immiscible PEO-*b*-PCL diblock or PCL-*b*-PEO-*b*-PCL triblock copolymers. The DSC and FTIR results demonstrate that phenolic preferentially forms hydrogen bonds with the PEO block rather than the PCL block. Moreover, the cooling results of DSC experiments show that the structural transition of PCL occurred through the T_f of PCL changing when phenolic resin was cured with HMTA. At relatively higher phenolic contents (>70 wt %), abundant phenolic becomes available to interact with both PEO and PCL through hydrogen bonding, and the blends become miscible disordered structures; furthermore, phenolic acts as a common solvent in this blend system. The self-organized mesoporous phenolic resin was observed only at 40−60 wt % phenolic content by an intriguing balance of the phenolic, PEO, and PCL contents. At lower phenolic contents (<30 wt % phenolic), insufficient phenolic resin was present to include the template PEO-*b*-PCL block copolymer and to form a complete mesoporous structure. As a result, a closed-loop mesoporous phenolic resin templated by EC block copolymers exists, which is similar to ternary polymer blends when all three binary pairs (B−A, B−C, and A−C) are individually miscible. A closed-loop immiscibility phase diagram has been observed due to the so-called "$\Delta\chi$" and "ΔK" effects. TEM images and SAXS analyses indicate that different compositions of phenolic result in different mesoporous structures through the mediation of hydrogen-bonding interactions. In addition, the large and long-range order of bicontinuous gyroid-type mesoporous carbon was obtained from mesoporous gyroid phenolic resin calcined at 800 °C under nitrogen.

ASSOCIATED CONTENT

Supporting Information. SAXS analyses, IR spectra, and TEM images. This material is available free of charge via the Internet at http://pubs.acs.org.

AUTHOR INFORMATION

Corresponding Author

*E-mail: kuosw@faculty.nsysu.edu.tw. Telephone: 886-7-5252000 ext. 4079. Fax: 886-7-5254099.

ACKNOWLEDGMENT

This work was supported financially by the National Science Council, Taiwan, Republic of China, under Contract No. NSC 100-2221-E-110-029-MY3 and NSC 100-2628-E-110-001.

REFERENCES

(1) Muthukumar, M.; Ober, C. K.; Thomas, E. L. *Science* **1997**, *277*, 1225.
(2) Stupp, S. I.; Braun, P. V. *Science* **1997**, *277*, 1242.
(3) Rodriguez-Hernandez, J.; Checot, F.; Gnanou, Y.; Lecommandoux, S. *Prog. Polym. Sci.* **2005**, *30*, 691.
(4) Hamley, I. U. *The Physics of Block Copolymers*; Oxford University Press: Oxford, U.K., 1998.
(5) Foerster, S.; Antonietti, M. *Adv. Mater.* **1998**, *10*, 195.
(6) Hadjichristidis, N.; Pispas, S.; Floudas, G. A. *Block Copolymers Synthetic Strategies, Physical Properties, and Applications*; John Wiley& Sons: Hoboken, NJ, 2003.
(7) Matsen, M. W. *Macromolecules* **1995**, *28*, 5765.
(8) Tanaka, T.; Hasegawa, H.; Hashimoto, T. *Macromolecules* **1991**, *24*, 240.

(9) Bendejacq, D.; Ponsinet, V.; Joanicot, M. *Macromolecules* **2002**, *35*, 6645.
(10) Lowenhaupt, B.; Steurer, A.; Hellmann, G. P.; Gallot, Y. *Macromolecules* **1994**, *27*, 908.
(11) Han, Y. K.; Pearce, E. M.; Kwei, T. K. *Macromolecules* **2000**, *33*, 1321.
(12) Jiang, M.; Xie, H. K. *Prog. Polym. Sci.* **1991**, *16*, 977.
(13) Zoelen, W. V.; Ekenstein, G. A. V.; Ikkala, O.; Brinke, G. T. *Macromolecules* **2006**, *39*, 6574.
(14) Huang, Y. Y.; Chen, H. L.; Hashimoto, T. *Macromolecules* **2003**, *36*, 764.
(15) Likhman, A. E.; Semenov, A. N. *Macromolecules* **1997**, *30*, 7273.
(16) Huang, Y. Y.; Hsu, J. Y.; Chen, H. L.; Hashimoto, T. *Macromolecules* **2007**, *40*, 3700.
(17) Matsushita, Y. *Macromolecules* **2007**, *40*, 771.
(18) Jinnai, H.; Hasegawa, H.; Nishikawa, Y.; Sevink, G. J. A.; Braunfeld, M. B.; Agard, D. A.; Spontak, R. J. *Macromol. Rapid Commun.* **2006**, *27*, 1424.
(19) Huang, P.; Zhu, L.; Cheng, S. Z. D.; Ge, Q.; Quirk, R. P.; Thomas, E. L.; Lotz, B.; Hsiao, B. S.; Liu, L. Z.; Yeh, F. J. *Macromolecules* **2001**, *34*, 6649.
(20) Vavasour, J. D.; Whitmore, M. D. *Macromolecules* **2001**, *34*, 3471.
(21) Maurer, W. W.; Bates, F. S.; Lodge, T. P. *J. Chem. Phys.* **1998**, *108*, 2989.
(22) Jeon, K. J.; Roe, R. J. *Macromolecules* **1994**, *27*, 2439.
(23) Shull, K. R.; Winey, K. I. *Macromolecules* **1992**, *25*, 2637.
(24) Bodycomb, J.; Yamaguchi, D.; Hashimoto, T. *Macromolecules* **2000**, *33*, 5187.
(25) Winey, K. I.; Thomas, E. L.; Fetters, L. J. *Macromolecules* **1992**, *25*, 2645.
(26) Xie, R.; Li, G.; Liu, C.; Jiang, B. *Macromolecules* **1996**, *29*, 4895.
(27) Lee, S.-H.; Char, K.; Kim, G. *Macromolecules* **2000**, *33*, 7072.
(28) Winey, K. I.; Thomas, E. L.; Fetters, L. J. *Macromolecules* **1992**, *25*, 422.
(29) Koizumi, S.; Hasegawa, H.; Hashimoto, T. *Macromolecules* **1994**, *27*, 7893.
(30) Yamaguchi, D.; Shiratake, S.; Hashimoto, T. *Macromolecules* **2000**, *33*, 8258.
(31) Mayes, A. M.; Russell, T. P.; Satijia, S. K.; Majkrzak, C. F. *Macromolecules* **1992**, *25*, 6523.
(32) Kuo, S. W. *Polym. Int.* **2009**, *58*, 455.
(33) Lee, H. F.; Kuo, S. W.; Huang, C. F.; Lu, J. S.; Chan, S. C.; Wang, C. F.; Chang, F. C. *Macromolecules* **2006**, *39*, 5458.
(34) Chen, W. C.; Kuo, S. W.; Jeng, U. S.; Chang, F. C. *Macromolecules* **2008**, *41*, 1401.
(35) Chen, W. C.; Kuo, S. W.; Lu, C. H.; Chang, F. C. *Macromolecules* **2009**, *42*, 3580–3590.
(36) Lin, I. H.; Kuo, S. W.; Chang, F. C. *Polymer* **2009**, *50*, 5276.
(37) Lu, C. H.; Kuo, S. W.; Chang, W. T.; Chang, F. C. *Macromol. Rapid Commun.* **2009**, *30*, 2121.
(38) Zhao, J. Q.; Pearce, E. M.; Kwei, T. K. *Macromolecules* **1997**, *30*, 7119.
(39) Kosonen, H.; Ruokolainen, J.; Nyholm, P.; Ikkala, O. *Polymer* **2001**, *42*, 9481.
(40) Kosonen, H.; Ruokolainen, J.; Nyholm, P.; Ikkala, O. *Macromolecules* **2001**, *34*, 3046.
(41) Dobrosielska, K.; Wakao, S.; Takano, A.; Matsushita, Y. *Macromolecules* **2008**, *41*, 7695.
(42) Dobrosielska, K.; Wakao, S.; Suzuki, J.; Noda, K.; Takano, A.; Matsushita, Y. *Macromolecules* **2009**, *42*, 7098.
(43) Chen, S. C.; Kuo, S. W.; Jeng, U. S.; Chang, F. C. *Macromolecules* **2010**, *43*, 1083.
(44) Hameed, N.; Guo, Q. *Polymer* **2008**, *49*, 922.
(45) Hameed, N.; Guo, Q. *Macromolecules* **2008**, *41*, 7596.
(46) Salim, N. V.; Hanley, T.; Guo, Q. *Macromolecules* **2010**, *43*, 7695.
(47) Salim, N. V.; Hameed, N.; Guo, Q. *J. Polym. Sci., Part B: Polym. Phys.* **2009**, *47*, 1894.
(48) Hameed, N.; Salim, N. V.; Guo, Q. *J. Chem. Phys.* **2009**, *131*, 214905.
(49) Hillmyer, M. A.; Lipic, P. M.; Hajduk, D. A.; Almdal, K.; Bates, F. S. *J. Am. Chem. Soc.* **1997**, *119*, 2749.
(50) Lipic, P. M.; Bates, F. S.; Hillmyer, M. A. *J. Am. Chem. Soc.* **1998**, *120*, 8963.
(51) Gong, W.; Zeng, K.; Wang, L.; Zheng, S. *Polymer* **2008**, *49*, 3318.
(52) Yi, F.; Zheng, S.; Liu, T. *J. Phys. Chem. B* **2009**, *113*, 11831.
(53) Zhuang, X.; Wan, Y.; Feng, C. M.; Shen, Y.; Zhao, D. Y. *Chem. Mater.* **2009**, *21*, 706.
(54) Yu, C. Z.; Fan, J.; Tian, B. Z.; Zhao, D. Y. *Chem. Mater.* **2004**, *16*, 889.
(55) Deng, Y. H.; Yu, T.; Wan, Y.; Shi, Y. F.; Meng, Y.; Gu, D.; Zhang, L. J.; Huang, Y.; Liu, C.; Wu, X. J.; Zhao, D. Y. *J. Am. Chem. Soc.* **2007**, *129*, 1690.
(56) Kosonen, H.; Ruokolainen, J.; Torkkeli, M.; Serimaa, R.; Nyholm, P.; Ikkala, O. *Macromol. Chem. Phys.* **2002**, *203*, 388.
(57) Zhang, F.; Meng, Y.; Gu, D.; Yan, Y.; Chen, Z.; Tu, B.; Zhao, D. *Chem. Mater.* **2006**, *18*, 5297.
(58) Huang, Y.; Cai, H.; Yu, T.; Zhang, F.; Zhang, F.; Meng, Y.; Gu, D.; Wan, Y.; Sun, X.; Tu, B.; Zhao, D. *Angew. Chem., Int. Ed.* **2007**, *46*, 1089.
(59) Valkama, S.; Nykanen, A.; Kosonen, H.; Ramani, R.; Tuomisto, F.; Engelhardt, P.; ten Brinke, G.; Ikkala, O.; Ruokolainen, J. *Adv. Funct. Mater.* **2007**, *17*, 183.
(60) Hu, D.; Xu, Z.; Zeng, K.; Zheng, S. *Macromolecules* **2010**, *43*, 2960.
(61) Kuo, S. W.; Lin, C. L.; Chang, F. C. *Macromolecules* **2002**, *35*, 278.
(62) Patterson, D. *Polym. Eng. Sci.* **1982**, *22*, 64.
(63) Zhang, H.; Bhagwagar, D. E.; Graf, J. F.; Paitner, P. C.; Coleman, M. M. *Polymer* **1994**, *35*, 5379.
(64) Jo, W. H.; Kwon, Y. K.; Kwon, I. H. *Macromolecules* **1991**, *24*, 4708.
(65) Kuo, S. W.; Chan, S. C.; Wu, H. D.; Chang, F. C. *Macromolecules* **2005**, *38*, 4729.
(66) Lin, H. C.; Kuo, S. W.; Huang, C. F.; Chang, F. C. *Macromol. Rapid Commun.* **2006**, *27*, 537.
(67) Huang, M. W.; Kuo, S. W.; Wu, H. D.; Chang, F. C.; Fang, S. Y. *Polymer* **2002**, *43*, 2479.
(68) Huang, C. F.; Kuo, S. W.; Lin, F. J.; Huang, W. J.; Wang, C. F.; Chen, W. Y.; Chang, F. C. *Macromolecules* **2006**, *39*, 300.
(69) Chiu, C. Y.; Hsu, W. H.; Yen, Y. J.; Kuo, S. W.; Chang, F. C. *Macromolecules* **2005**, *38*, 6640.
(70) Kuo, S. W.; Huang, C. F.; Chang, F. C. *J. Polym. Sci.: Polym. Phys.* **2001**, *39*, 1348.
(71) Kuo, S. W.; Chan, S. C.; Chang, F. C. *J. Polym. Sci.: Polym. Phys.* **2004**, *42*, 117.
(72) Kuo, S. W.; Huang, W. J.; Huang, C. F.; Chan, S. C.; Chang, F. C. *Macromolecules* **2004**, *37*, 4164.
(73) Kuo, S. W.; Liu, W. P.; Chang, F. C. *Macromol. Chem. Phys.* **2005**, *206*, 2307.
(74) Huang, K. W.; Tsai, L. W.; Kuo, S. W. *Polymer* **2009**, *50*, 4876.
(75) Moskala, E. J.; Varnell, D. F.; Coleman, M. M. *Polymer* **1985**, *26*, 228.
(76) Coleman, M. M.; Graf, J. F.; Painter, P. C. *Specific Interactions and the Miscibility of Polymer Blends*; Technomic Publishing: Lancaster, PA, 1991.
(77) Coleman, M. M.; Painter, P. C. *Miscible Polymer Blend-Background and Guide for Calculations and Design*; DEStech Publications, Inc.: Lancaster, PA, 2006.
(78) Zhong, Z.; Guo, Q. *Polymer* **1997**, *38*, 279.
(79) Chen, H. L.; Hsiao, S. C.; Lin, T. L.; Yamauchi, K.; Hasegawa, H.; Hashimoto, T. *Macromolecules* **2001**, *34*, 671.
(80) Chen, H. L.; Wu, J. C.; Lin, T. L.; Lin, J. S. *Macromolecules* **2001**, *34*, 6936.
(81) Loo, Y. L.; Register, R. A.; Ryan, A. J.; Dee, G. T. *Macromolecules* **2001**, *34*, 8968.

(82) Chen, H. L.; Lin, S. Y.; Huang, Y. Y.; Chiu, F. C.; Liou, W.; Lin, J. S. *Macromolecules* **2002**, *35*, 9434.
(83) Xu, J. T.; Turners, S. C.; Fairclough, J. P. A.; Mai, S. M.; Ryan, A. J.; Chaibundit, C.; Booth, C. *Macromolecules* **2002**, *35*, 3614.
(84) Hsu, J. Y.; Hsieh, I. F.; Nandan, B.; Chiu, F. C.; Chen, J. H.; Jeng, U. S.; Chen, H. L. *Macromolecules* **2007**, *40*, 5014.
(85) Pomposo, J. A.; Calahorra, E.; Eguiazabal, I.; Cortazar, M. *Macromolecules* **1993**, *26*, 2104.
(86) Lin, C. L.; Chen, W. C.; Kuo, S. W.; Chang, F. C. *Polymer* **2006**, *47*, 3436.
(87) Harkin, W. D.; Jura, G. *J. Am. Chem. Soc.* **1944**, *66*, 1366.
(88) Sing, K. S. W.; Everett, D. H.; Hual, R. A. W.; Pierotti, R. A.; Rouquerol, J.; Siemieniewska, T. *Pure Appl. Chem.* **1985**, *57*, 603.
(89) Deng, Y.; Liu, C.; Gu, D.; Yu, T.; Tu, B.; Zhao, D. *J. Mater. Chem.* **2008**, *18*, 91.
(90) Rumplecker, A.; Kleitz, F.; Salabas, E. L.; Schuth, F. *Chem. Mater.* **2007**, *19*, 485.